Spectral fractionation detection of gold nanorod contrast agents using optical coherence tomography

Yali Jia,[1,4] Gangjun Liu,[1,4] Andrew Y. Gordon,[2] Simon S. Gao,[1] Alex D. Pechauer,[1] Jonathan Stoddard,[1] Trevor J. McGill,[1] Ashwath Jayagopal,[3] and David Huang[1,*]

[1]*Casey Eye Institute, Oregon Health & Science University, Portland, Oregon 97239, USA*
[2]*Department of Molecular Physiology and Biophysics, Vanderbilt University Medical Center, Nashville, Tennessee 37232, USA*
[3]*Department of Ophthalmology and Visual Sciences, Vanderbilt Eye Institute, Nashville, Tennessee 37232, USA*
[4]*Co-first authors*
[*]*huangd@ohsu.edu*

Abstract: We demonstrate the proof of concept of a novel Fourier-domain optical coherence tomography contrast mechanism using gold nanorod contrast agents and a spectral fractionation processing technique. The methodology detects the spectral shift of the backscattered light from the nanorods by comparing the ratio between the short and long wavelength halves of the optical coherence tomography signal intensity. Spectral fractionation further divides the halves into sub-bands to improve spectral contrast and suppress speckle noise. Herein, we show that this technique can detect gold nanorods in intralipid tissue phantoms. Furthermore, cellular labeling by gold nanorods was demonstrated using retinal pigment epithelial cells *in vitro*.

©2015 Optical Society of America

OCIS codes: (170.4500) Optical coherence tomography; (170.3880) Medical and biological imaging.

References and links

1. D. Huang, E. A. Swanson, C. P. Lin, J. S. Schuman, W. G. Stinson, W. Chang, M. R. Hee, T. Flotte, K. Gregory, C. A. Puliafito, and J. G. Fujimoto, "Optical coherence tomography," Science **254**(5035), 1178–1181 (1991).
2. W. Drexler and J. G. Fujimoto, eds., *Optical Coherence Tomography: Technology and Applications* (Springer-Verlag, 2008).
3. W. Drexler, "Ultrahigh-resolution optical coherence tomography," J. Biomed. Opt. **9**(1), 47–74 (2004).
4. S. A. Boppart, A. L. Oldenburg, C. Xu, and D. L. Marks, "Optical probes and techniques for molecular contrast enhancement in coherence imaging," J. Biomed. Opt. **10**(4), 41208 (2005).
5. Z. Yaqoob, E. McDowell, J. Wu, X. Heng, J. Fingler, and C. Yang, "Molecular contrast optical coherence tomography: A pump-probe scheme using indocyanine green as a contrast agent," J. Biomed. Opt. **11**(5), 054017 (2006).
6. K. M. Au, Z. Lu, S. J. Matcher, and S. P. Armes, "Polypyrrole nanoparticles: a potential optical coherence tomography contrast agent for cancer imaging," Adv. Mater. **23**(48), 5792–5795 (2011).
7. T. S. Troutman, J. K. Barton, and M. Romanowski, "Optical coherence tomography with plasmon resonant nanorods of gold," Opt. Lett. **32**(11), 1438–1440 (2007).
8. A. L. Oldenburg, M. N. Hansen, D. A. Zweifel, A. Wei, and S. A. Boppart, "Plasmon-resonant gold nanorods as low backscattering albedo contrast agents for optical coherence tomography," Opt. Express **14**(15), 6724–6738 (2006).
9. C. Yang, L. E. McGuckin, J. D. Simon, M. A. Choma, B. E. Applegate, and J. A. Izatt, "Spectral triangulation molecular contrast optical coherence tomography with indocyanine green as the contrast agent," Opt. Lett. **29**(17), 2016–2018 (2004).
10. T. S. Kim, S. J. Jang, N. Oh, Y. Kim, T. Park, J. Park, and W. Y. Oh, "Dual-wavelength band spectroscopic optical frequency domain imaging using plasmon-resonant scattering in metallic nanoparticles," Opt. Lett. **39**(10), 3082–3085 (2014).
11. N. R. Jana, L. Gearheart, and C. J. Murphy, "Seed-mediated growth approach for shape-controlled synthesis of spheroidal and rod-like gold nanoparticles using a surfactant template," Adv. Mater. **13**(18), 1389–1393 (2001).

#224761 - $15.00 USD Received 10 Oct 2014; revised 14 Jan 2015; accepted 5 Feb 2015; published 11 Feb 2015
© 2015 OSA

12. E. M. Barnett, B. Elangovan, K. E. Bullok, and D. Piwnica-Worms, "Selective cell uptake of modified Tat peptide-fluorophore conjugates in rat retina in ex vivo and in vivo models," Invest. Ophthalmol. Vis. Sci. **47**(6), 2589–2595 (2006).
13. Y. Nakamura, Y. Tsuru, M. Fujii, Y. Taga, A. Kiya, N. Nakashima, and Y. Niidome, "Sensing of oligopeptides using localized surface plasmon resonances combined with Surface-Assisted Laser Desorption/Ionization Time-of-Flight Mass Spectrometry," Nanoscale **3**(9), 3793–3798 (2011).
14. Y. Jia, O. Tan, J. Tokayer, B. Potsaid, Y. Wang, J. J. Liu, M. F. Kraus, H. Subhash, J. G. Fujimoto, J. Hornegger, and D. Huang, "Split-spectrum amplitude-decorrelation angiography with optical coherence tomography," Opt. Express **20**(4), 4710–4725 (2012).
15. K. S. Lee and M. A. El-Sayed, "Dependence of the enhanced optical scattering efficiency relative to that of absorption for gold metal nanorods on aspect ratio, size, end-cap shape, and medium refractive index," J. Phys. Chem. B **109**(43), 20331–20338 (2005).
16. B. C. Rostro-Kohanloo, L. R. Bickford, C. M. Payne, E. S. Day, L. J. Anderson, M. Zhong, S. Lee, K. M. Mayer, T. Zal, L. Adam, C. P. Dinney, R. A. Drezek, J. L. West, and J. H. Hafner, "The stabilization and targeting of surfactant-synthesized gold nanorods," Nanotechnology **20**(43), 434005 (2009).
17. P. K. Jain, S. Eustis, and M. A. El-Sayed, "Plasmon coupling in nanorod assemblies: optical absorption, discrete dipole approximation simulation, and exciton-coupling model," J. Phys. Chem. B **110**(37), 18243–18253 (2006).
18. W. Zhou, X. Liu, and J. Ji, "Fast and selective cancer cell uptake of therapeutic gold nanorods by surface modifications with phosphorylcholine and Tat," J. Mater. Chem. **22**(28), 13969–13976 (2012).
19. C. Xu, P. Carney, and S. Boppart, "Wavelength-dependent scattering in spectroscopic optical coherence tomography," Opt. Express **13**(14), 5450–5462 (2005).
20. A. L. Oldenburg, M. N. Hansen, T. S. Ralston, A. Wei, and S. A. Boppart, "Imaging gold nanorods in excised human breast carcinoma by spectroscopic optical coherence tomography," J. Mater. Chem. **19**(35), 6407 (2009).
21. A. de la Zerda, S. Prabhulkar, V. L. Perez, M. Ruggeri, A. S. Paranjape, F. Habte, S. S. Gambhir, and R. M. Awdeh, "Optical coherence contrast imaging using gold nanorods in living mice eyes," Clin. Experiment. Ophthalmol., http://europepmc.org/abstract/med/24533647 (2014).
22. J. M. Tucker-Schwartz, T. A. Meyer, C. A. Patil, C. L. Duvall, and M. C. Skala, "In vivo photothermal optical coherence tomography of gold nanorod contrast agents," Biomed. Opt. Express **3**(11), 2881–2895 (2012).
23. A. L. Oldenburg, R. K. Chhetri, J. M. Cooper, W. C. Wu, M. A. Troester, and J. B. Tracy, "Motility-, autocorrelation-, and polarization-sensitive optical coherence tomography discriminates cells and gold nanorods within 3D tissue cultures," Opt. Lett. **38**(15), 2923–2926 (2013).
24. G. S. He, J. Zhu, K.-T. Yong, A. Baev, H.-X. Cai, R. Hu, Y. Cui, X.-H. Zhang, and P. N. Prasad, "Scattering and absorption cross-section spectral measurements of gold nanorods in water," J. Phys. Chem. C **114**(7), 2853–2860 (2010).
25. L. Qiu, T. A. Larson, E. Vitkin, L. Guo, E. B. Hanlon, I. Itzkan, K. V. Sokolov, and L. T. Perelman, "Gold nanorod light scattering labels for biomedical imaging," Biomed. Opt. Express **1**(1), 135–142 (2010).

1. Introduction

Optical coherence tomography (OCT) is a noninvasive and nondestructive imaging modality that is capable of providing micron-scale axial resolution for *in vitro* and *in vivo* imaging applications through the use of low-coherence interferometry [1]. It has been successfully integrated into pre-clinical and clinical research in the fields of ophthalmology, dermatology, cardiology, otolaryngology, and oncology, among others [2]. OCT primarily relies on variations in optical scattering and absorption between tissue layers and cell types. As an example, retinal nerve fibers and pigment epithelium are more reflective than their surrounding tissue, and this type of endogenous tissue contrast is sufficient to delineate nearly all retinal sublayers that are identifiable in histology [3]. A long-standing limitation of OCT, however, has been the lack of an effective and practical contrast agent capable of cellular and molecular labeling. OCT cannot utilize typical fluorescent labeling because the fluorescence absorption and emission process destroys the coherence required for OCT [4]. As a result, the search for and development of contrast agents for implementation with OCT is of significant interest.

In this study, we sought to develop a gold nanorod (GNR) contrast agent to label cells for OCT imaging. The eventual goal was to label stem cells that could be used in the treatment of retinal disease. To demonstrate feasibility, we used cultured retinal pigment epithelial (RPE) cells for labeling, and low concentration intralipid to simulate the semitransparent tissue of the retina. To enhance contrast, we engineered GNR to have spectrally-encoded backscatter/reflectance by tuning their surface plasmon resonance (SPR) peak to a wavelength that is shifted to one side of the OCT spectral band. The spectrally shifted GNR

#224761 - $15.00 USD Received 10 Oct 2014; revised 14 Jan 2015; accepted 5 Feb 2015; published 11 Feb 2015
© 2015 OSA

backscatter/reflection can then be detected by a novel type of spectroscopic analysis that we call spectral fractionation. We demonstrate a proof of concept for cellular labeling *in vitro*. Human retina was also imaged *in vivo* with the same technique to demonstrate that background tissue noise could be suppressed with the spectral fractionation algorithm.

It should be noted that our goal was to enhance contrast by means of characteristic spectral shift in the backscattered OCT signal. This differed from previous methods that enhanced contrast by means of characteristic spectral OCT signal shift due to absorption effects from indocyanine green dye [5] or nanoparticles [6–8]. The reasoning was that absorption effects would be too small for small clusters of GNR in a sparse concentration of cells to produce useful contrast. Absorptive contrast worked in previous experiments where broad regions of turbid tissue were labeled with a high concentration of dye [9, 10], but that would not be useful in our intended application.

2. Materials and methods

2.1 OCT systems

Imaging experiments were conducted on a commercial spectral Fourier-domain OCT system (RTVue-XR, Optovue, Fremont, CA) and a custom-built swept-source OCT system. The commercial system has a center wavelength of ~840 nm with a full-width-half-maximum (FWHM) bandwidth of 45 nm and a 70 kHz axial scan repetition rate. It has an axial resolution of 5 µm in tissue. The system was customized to allow saving of the raw spectral data. A 30 mm lens was used for focusing the light on to the sample. The swept-source OCT system has a center wavelength of 1050 nm with a FWHM bandwidth of ~100 nm and a speed of 100 kHz. It has an axial resolution of 7.1 µm in air and a lateral resolution of 19 µm.

2.2 GNR synthesis

Cetyl trimethylammonium bromide (CTAB) coated gold nanorods were synthesized according to previously published procedures [11]. Gold nanorods feature characteristic SPR that is tunable by their aspect ratio. The SPR of 10 nm diameter sized gold nanorods were adjusted to peak values of 900 nm and 980 nm by tuning their length dimensions to 50 nm and 59 nm, respectively. Nanorods were then coated with 1000 molecular weight polyethylene glycol (PEG) *via* incubation of nanorods with 10-fold molar excess of thiol-PEG-Tat peptide (Laysan Bio, Inc., Arab, AL) in PBS (pH = 7.4) for 12 hours with gentle mixing on a tube rotator. The Tat peptide featured D- amino acids and consisted of the sequence RKKRRORRR as previously reported [12]. Excess PEG-Tat was removed by 6 rounds of centrifugation at 21,000X G with rinsing using PBS. Displacement of CTAB with PEG residues was monitored using zeta potential analysis and surface assisted laser desorption ionization mass spectrometry as previously described for gold nanorod characterization [13]. All zeta potential measurements were taken with a Zetasizer Nano ZS90 (Malvern Instruments, Malvern, UK). Furthermore, post-conjugation of PEG-Tat, nanorods were characterized for preservation of size using transmission electron microscopy (Fig. 1(a)). The extinction spectra of the stock GNR solution with a concentration of 5×10^{11} nanorods/mL were also collected (Fig. 1(b)).

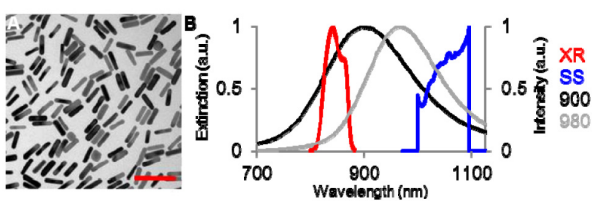

Fig. 1. (a) Transmission electron micrograph of monodisperse GNR coated with PEG and Tat cell internalization peptide. Scale bar is 100 nm. (b) Normalized extinction spectra of the

#224761 - $15.00 USD Received 10 Oct 2014; revised 14 Jan 2015; accepted 5 Feb 2015; published 11 Feb 2015
© 2015 OSA

synthesized GNR with SPR at 900 nm (10 × 50 nm, black) and 980 nm (10 × 59 nm, gray). Normalized intensity spectra of the commercial OCT (XR, red) and swept-source OCT systems (SS, blue).

2.3 Transmission measurement

The swept-source laser with center wavelength of 1050 nm (Axsun Technologies Inc., Billerica, MA) was used as the light source, and the sample was inserted between two fiber collimators. The laser spectrum was measured with an optical spectrum analyzer (AQ6370B, Yokogawa, Sugar Land, TX) after it passed through a cuvette holding the sample (Fig. 2(a)). The cuvette has a volume of 2 mL with a single-trip optical pathlength of 4 mm. To test transmission of the stock GNR (with SPR at 980 nm) solution (5×10^{11} nanorods/mL), deionized water (0.5 mL) was first added to the cuvette to establish a baseline measurement. The water was then removed and replaced with stock GNR solution. A second measurement was taken. This procedure was repeated 5 times, and average transmission spectrums were calculated. To test transmission through dilute GNR solution, deionized water was added to the cuvette to establish a baseline measurement. GNR (with SPR at 980 nm) stock solution was then added to the deionized water to produce a dilute GNR solution with a concentration of 5×10^{10} nanorods/mL. A second measurement was then taken. This procedure was again repeated 5 times, and average transmission spectrums were calculated.

2.4 Phantom preparation

Tissue phantoms (5 mL) of intralipid, GNR, and GNR-in-intralipid were all prepared by serial dilution from stock solutions and imaged in 10 mL test tubes using OCT. Intralipid 20% stock solution (Intralipid 20%, emulsion, Sigma-Aldrich, St. Louis, MO) was diluted down to 0.1% using molecular grade water. GNR stock solution (5×10^{11} nanorods/mL) was serially diluted using molecular grade water to 5×10^{10} nanorods/mL. The GNR-in-intralipid solution was prepared by first diluting the stock intralipid solution to 0.1%. This solution was then used to dilute stock GNR solution, resulting in a final 0.1% intralipid sample with 5×10^{10} nanorods/mL.

2.5 Cell preparation

Gelatin-coated plates with no cells, unlabeled RPE cells, and GNR-labeled RPE cells were imaged *in vitro* using OCT. Cell plates containing approximately 500,000 retinal pigment epithelial (RPE) stem cells were incubated with 1×10^9 Tat-coated GNR for 4 hours at 37°C on an agitator (at 30 RPM). Afterwards, the cell plates were washed free of GNR by triplicate rinsing with warmed HBSS, thus allowing for only GNR taken up by RPE cells to remain. Cells were then trypsinized, centrifuged, and fixed using 1 mL 10% neutral buffered formalin at room temp for 10 min.

Prior to the addition of labeled cells, a basal layer was first prepared in the wells that would contain no cells, labeled cells, or unlabeled cells using 3 mL of 1% gelatin. This created a depth of approximately 300 μm above the plastic bottom of the well plate for imaging purposes. Cells were then resuspended in an additional 2 mL of 1% gelatin. This was subsequently added to the previously solidified, gelatin coated plates. This provided an additional depth of approximately 200 μm for imaging.

2.6 OCT of human retina

Normal human retinas were imaged by the 840 nm spectral OCT system. The protocol was approved by the Institutional Review Board (IRB). The subject's head was stabilized by chin and forehead rests and guided by a flashing internal fixation target. Ten consecutive B-scans were acquired in one session. Each B-scan contained 2300 A-scans over 3.1 mm. The same scan protocol was used for scanning phantoms and tissues.

#224761 - $15.00 USD Received 10 Oct 2014; revised 14 Jan 2015; accepted 5 Feb 2015; published 11 Feb 2015
© 2015 OSA

2.7 Theory for spectral fractionation detection of spectrally-encoded GNR contrast agents

The OCT signal is derived from the interferogram between light returned from the reference arm and backscattered/reflected light from the sample. For a Fourier-domain OCT system, neglecting the DC part, the detected spectral interferogram is given by

$$I(k) = \mathrm{Re}\left\{\int S(k)\cdot r_s(k,z)\cdot r_r(k)\cdot \exp(-i2k\Delta z)dz\right\} \tag{1}$$

where $S(k)$ is the power spectrum of the OCT light source, $r_r(k)$ is the spectral amplitude reflectivity of the reference mirror, $r_s(k,z)$ is the spectral amplitude reflectivity of the sample backscattered/reflected light at depth z, k is the wavenumber, and Δz is the path difference between sample and reference mirror. The depth information is calculated by performing an inverse Fourier transformation of Eq. (1) with respect to k

$$I(z) = \mathbb{F}^{-1}\left\{I(k)\right\} \tag{2}$$

where $\mathbb{F}^{-1}$ is the inverse Fourier transform. For a typical OCT setup, $r_r(k)$ is constant and wavelength independent because a mirror is usually used in the reference arm. Biological tissues can have wavelength dependent absorption and scattering properties, and therefore, the OCT sample arm reflectance $r_s(k,z)$ is generally wavelength dependent. The addition of GNR contrast agents will produce localized, systemic spectral shifts that can be used to identify them. Here, we detect this spectral shift using the ratio between the short and long wavelength halves (SLoW Ratio) of the OCT signal amplitude. In order to improve the signal-to-noise ratio, the short/long band may be further split into several sub-bands through a window function and repeated B-scans can be used to reduce speckle noise. Through this spectral fractionation, the SLoW ratio will be

$$SLoW(z) = \frac{\sum_{j=1}^{M}\sum_{si=1}^{N}\left|I_{j,si}(z)\right|}{\sum_{j=1}^{M}\sum_{li=1}^{N}\left|I_{j,li}(z)\right|} = \frac{\sum_{j=1}^{M}\sum_{si=1}^{N}\left|\mathbb{F}^{-1}\left\{I_j(k)\cdot G_{si}(k)\right\}\right|}{\sum_{j=1}^{M}\sum_{li=1}^{N}\left|\mathbb{F}^{-1}\left\{I_j(k)\cdot G_{li}(k)\right\}\right|} \tag{3}$$

where M is the number of repeated B-scans, N is the number of sub-bands for short/long band, $I_j(k)$ is the acquired interferogram from the j th B-scan, $G_{si}(k)$ and $G_{li}(k)$ are the Gaussian window functions used for the i th sub-band in the short and long band.

2.8 Image analysis

The collected data were analyzed with the spectral fractionation OCT processing technique. The raw interferogram from any single position was first separated into short and long wavelength halves around the center wavelength of OCT system. Each half was then further spectrally fractionated into four sub-bands, similar to what has been described previously [14]. The OCT signal from each sub-band was then Fourier-transformed to obtain A-scans as in conventional Fourier-domain OCT algorithms. The resulting signal intensities from the spectral bands were averaged together to obtain short and long wavelength OCT depth profiles. This processing was done for all A-scans in 10 consecutive B-frame images acquired at the same location. The 10 sets of results were averaged.

To evaluate the spectral shift of the OCT signal as a result of the GNR, the SLoW intensity ratio was evaluated for each pixel with signal strength above an intensity threshold. The intensity threshold was defined as the mean plus three times the standard deviation (SD) of the signal at a noise region above the sample of interest. The multi-frame and multi-band imaging/processing steps were taken to suppress speckle noise and decrease the spread of the

#224761 - $15.00 USD Received 10 Oct 2014; revised 14 Jan 2015; accepted 5 Feb 2015; published 11 Feb 2015
© 2015 OSA

SLoW ratio in tissue. When GNR with SPR at 900 nm (Fig. 1(b)) are imaged with the 840 nm commercial OCT system, the longer wavelength bands will have stronger backscattered/reflected signals. Thus, when the SLoW ratio is presented on a decibel (dB) scale, a negative value denotes the potential presence of GNR. Conversely, when GNR with SPR at 980 nm (Fig. 1(b)) are imaged with the 1050 nm swept-source OCT system, the shorter wavelength bands will have stronger backscattered/reflected signals. Thus, a positive value of the SLoW ratio presented on a dB scale denotes the potential presence of GNR.

3. Results

3.1 Transmission measurement

This work was based on previous analytical models which predict an increase in both scattering and absorption at SPR peaks [15]. Since an OCT contrast agent detection scheme based on backscattering/reflectance was preferred over absorption, an initial experiment was devised to test GNR absorption in stock (5×10^{11} nanorods/mL) and diluted solutions (5×10^{10} nanorods/mL). The setup is shown in Fig. 2(a). The stock GNR solution showed significant attenuation and spectral changes due to absorption (Fig. 2(b)), while the dilute GNR solution had essentially the same transmission spectra as deionized water, with a difference of less than 0.13% (Fig. 2(c)). This demonstrates that the effect of absorption was negligible at the dilute GNR concentration.

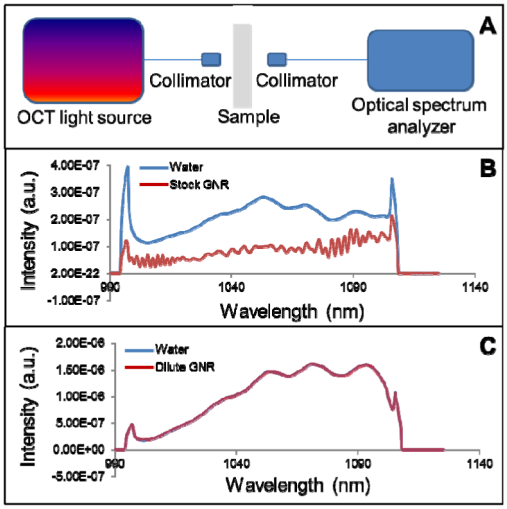

Fig. 2. (a) Schematic of the experimental setup. (b) Transmission spectra of water and stock GNR solution (5×10^{11} nanorods/mL) over a 4 mm pathlength. (c) Transmission spectra of water and dilute GNR solution (5×10^{10} nanorods/mL) overlapped with a negligible difference.

3.2 GNR aggregation

OCT imaging of dilute GNR solutions revealed aggregation, indicated by the presence of discrete, sparse scatterers. GNR with two different surface functionalizations were used in the following studies. The initial work utilized GNR functionalized with surface CTAB, which relied on creating sufficient electrostatic repulsion between GNRs to prevent aggregation [16]. However, following the 1:10 dilution of these CTAB-coated GNR in deionized water, there was insufficient CTAB in solution to maintain GNR stability. Evidence for this finding included negative shifts in the peak absorbance (SPR) of these nanorods following dilution (Table 1), consistent with side-by-side aggregation [17]. Zeta potential measurements of the GNR solutions provided additional evidence for the loss of CTAB from the GNR surface.

#224761 - $15.00 USD Received 10 Oct 2014; revised 14 Jan 2015; accepted 5 Feb 2015; published 11 Feb 2015
© 2015 OSA

Following dilution, the zeta potential of the 10 × 50 nm GNRs was + 1.1 mV, compared to + 53.5 mV prior to dilution (Table 1). Likewise, the zeta potential of the 10 × 59 nm GNRs was also reduced following dilution. The second type of GNR used was PEG-Tat coated and was meant to be internalized by cells. Previous work indicated that GNR coated with the Tat peptide would be internalized intracellularly into vesicles and that they would aggregate during this process [18]. Henceforth, dilute GNR refers to GNR at a concentration of 5×10^{10} nanrods/mL.

Table 1. Measurements of the SPR peaks and zeta potentials of CTAB-coated GNR

Sample	Concentration	SPR Peak (nm)	Zeta Potential (mV)
CTAB 10 × 50 nm GNR (stock)	5×10^{11} nanorods/mL	900	53.5
CTAB 10 × 50 nm GNR (dilute)	5×10^{10} nanorods/mL	870	1.1
CTAB 10 × 59 nm GNR (stock)	5×10^{11} nanorods/mL	980	36.1
CTAB 10 × 59 nm GNR (dilute)	5×10^{10} nanorods/mL	963	13.7

3.3 Calculation of spectral shift from theory

To test the theoretical framework, simulation was used to determine the expected SLoW ratio spectral shift when using the 840 nm spectral OCT system and dilute GNR with SPR at 870 nm. To calculate the SLoW ratio using Eq. (3), we used the measured light source spectrum and the scattering spectrum of the GNR. Absorption was deemed negligible based on the transmission measurement of dilute GNR. The scattering spectrum was based on the measured extinction spectrum, which have the same shape according to literature [15]. Normalization was performed to take the light source spectrum into consideration so that a SLoW ratio of zero dB would be found for wavelength independent samples. The numerically simulated normalized SLoW ratio was found to be −0.68 dB when using 4 sub-bands in the short/long bands. This spectral shift was approximately proportional to the OCT spectral bandwidth assuming a linear slope of GNR SPR.

3.4 GNR detection in tissue phantoms

Tissue phantoms were subsequently used to test the detection methodology. B-scan images of 0.1% intralipid, dilute GNR with SPR at 870 nm, and dilute GNR mixed with intralipid were taken on the 840 nm commercial OCT system. The 0.1% intralipid concentration was chosen to represent retinal tissue, which is more transparent than most tissues. A layer of aggregated GNR was seen at the test tube wall interface. The images were processed using the spectral fractionation technique described in Sections 2.7-2.8, and the SLoW ratios were calculated. We also processed the images without splitting the short/long wavelength bands into 4 sub-bands (Fig. 3(a)) to show the effect of that step. Histogram distribution plots of the SLoW ratios on a dB scale for the intralipid and GNR samples were generated without taking into account the aggregated layer at the test tube wall interface (Fig. 3(b)). The histograms were normalized to the total number of pixels in the B-scan which met the initial intensity threshold. The intralipid showed a normal distribution centered on zero (Fig. 3(b)). Without the spectral fractionation sub-band split, the SD of the intralipid SLoW distribution was greater, 0.54 dB versus 0.32 dB. The dilute GNR had a SLoW ratio mean of −0.5 dB without fractionation and −0.66 dB with. The latter value was in agreement with the simulated value of −0.68 dB.

We then defined the SLoW ratio shift between the distribution plots of the two samples as the difference between the means (Fig. 3(b)). Without the spectral fractionation sub-band split, the mean SLoW ratio shift from the GNR sample was within one SD of the intralipid SLoW distribution. Using a cutoff of 3.09 SD or −1.67 dB (Fig. 3(b), blue line) as the criteria

#224761 - $15.00 USD Received 10 Oct 2014; revised 14 Jan 2015; accepted 5 Feb 2015; published 11 Feb 2015
© 2015 OSA

of identifying the presence of GNR, 1% of the SLoW signal from the GNR sample remained. With spectral fractionation, the mean from the GNR sample showed a SLoW ratio with a mean ~2 SD less than that of the intralipid distribution. Using a cutoff of 3.09 SD or −1.0 dB SLoW ratio as the cutoff (blue line), the GNR signal could be cleanly separated from the intralipid signal. Specifically, 18% of the SLoW signal from the GNR sample was less than −1 dB compared to only 0.1% from the intralipid sample. The improved contrast with the spectral fractionation algorithm is clearly seen when we represented the SLoW ratios on a color scale in cross-sectional OCT images of the GNR sample (Fig. 3(c)). Aggregated GNR at the test tube wall produced a similar amount of red-shifted pixels with some blue-shifted pixels with or without spectral fractionation.

To facilitate measurement and comparison of the effectiveness of the contrast mechanism, we introduce the term spectral contrast S_c and define it as

$$S_c = \frac{M_{GNR} - M_S}{\sigma_s} \tag{4}$$

where M_{GNR} is the mean SLoW ratio on a dB scale from the GNR sample distribution plot, M_s is the mean from the GNR free sample, and σ_s the standard deviation from the GNR free sample. M_{GNR} - M_s represents the SLoW ratio shift. A greater spectral contrast value would indicate an enhanced ability to identify the presence of GNR within the mixture. Without spectral fractionation, the spectral contrast of 0.1% intralipid and GNR with SPR at 870 nm was then 0.93. With spectral fractionation, the spectral contrast improves to 2.06. It should be noted that the narrow spectral bandwidth of the sub-bands extends the coherence length. When the absolute values of the sub-sums are averaged, this suppresses the spectral speckle noise. It is possible that higher N could further suppress speckle noise, but that comes at the cost of worse spatial resolution in depth. We only used 4 sub-bands with FWHM bandwidth of 15 nm to preserve a 12 micron depth resolution which is at the cellular scale that we wished to image.

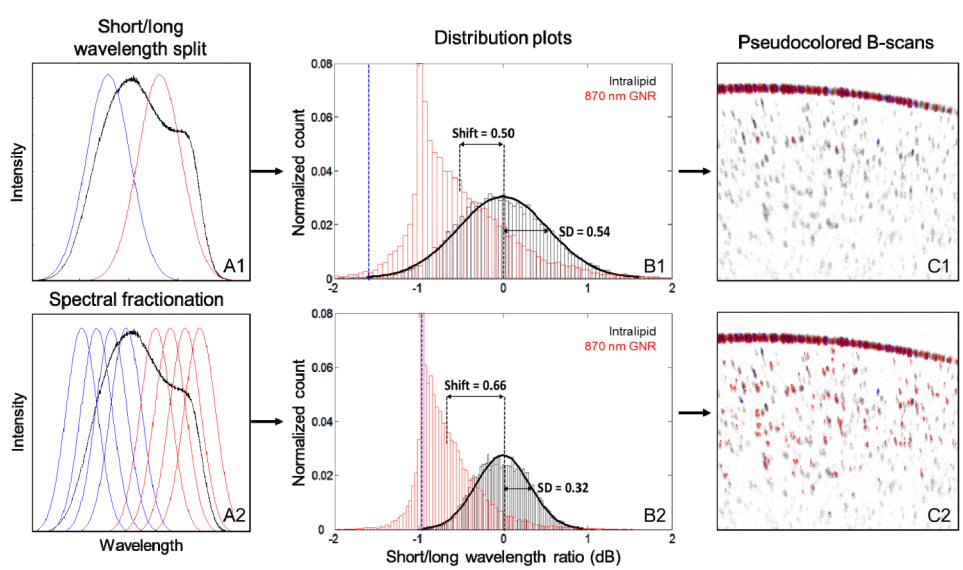

Fig. 3. (A1) Raw interferogram (black) was split into short (blue) and long (red) wavelength halves. (A2) Each half was divided into four narrower bands using Gaussian filters to improve detection. (B1) Histogram distribution plot showing the spectral shift of the OCT signal from 0.1% intralipid (tissue phantom) and dilute GNR with SPR at 870 nm (5×10^{10} nanorods/mL) without spectral fractionation. (B2) The same data processed with spectral fractionation. The spectral shift was determined by the ratio between the intensity of short (<840 nm) and long

#224761 - $15.00 USD Received 10 Oct 2014; revised 14 Jan 2015; accepted 5 Feb 2015; published 11 Feb 2015
© 2015 OSA

(>840 nm) wavelength components of the OCT signal and converted to a dB scale. Intralipid samples (black) showed normal distributions centered on zero. The GNR samples showed SLoW ratios with means within 1 SD (B1) or ~2 SD (B2) less than that of the intralipid distribution. (C1) Cross-sectional OCT images of dilute GNR in solution with SLoW ratios calculated without spectral fractionation and represented on a color scale. SLoW ratio (dB) more than 3.09 SD red shifted from the intralipid reference mean (blue line in (B1)) is shown in red, SLoW ratio more than 3.09 SD blue shifted is shown in blue. OCT signal intensity is shown on an inverse gray scale. Aggregation at the test tube wall produced red-shifted pixels with some blue-shifted pixels. Below the test tube interface, 1% of the GNR signal could be detected. (C2) Cross-sectional OCT image with SLoW ratios calculated with spectral fractionation. Below the aggregation at the test tube interface, 18% of the GNR signal could be detected.

Using the ± 1 dB cutoffs to define the separation between intralipid and GNR, B-scan images from the intralipid, GNR with SPR at 870 nm, and GNR mixed with intralipid samples were analyzed. Due to speckle noise, the intralipid (Fig. 4(a)) showed a few colored pixels. The red shifted GNR signal could be clearly visualized by itself (Fig. 4(b)) and when mixed with intralipid (Fig. 4(c)). The discrete scatterers in the OCT image of the dilute GNR solution indicated aggregation. A layer of GNR aggregate is evident in the interface between the suspension and test tube wall in Fig. 4(b) and 4(c). This layer showed intense backscattering with the expected red shift. Blue-shifted pixels were also seen and may be due to speckle effects within large aggregates.

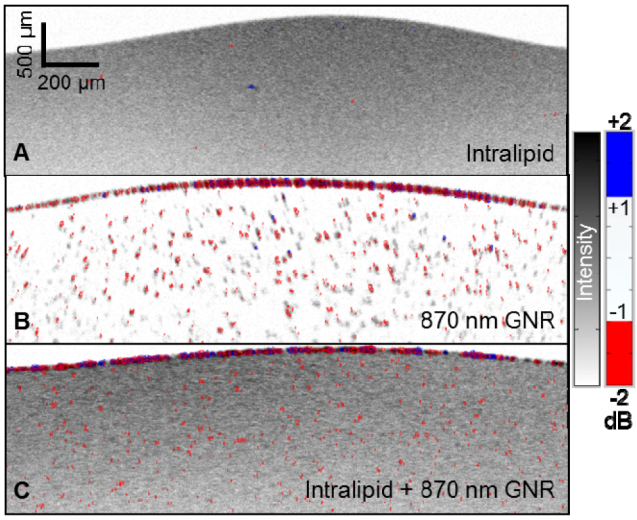

Fig. 4. OCT images of (a) 0.1% intralipid, (b) dilute GNR with SPR at 870 nm, and (c) dilute GNR-in-intralipid. The OCT signal intensity is shown on an inverse gray scale, and the SLoW ratio is color-coded with cutoffs set at ± 3.09 SD (± 1 dB) of the spectral distribution of intralipid (Fig. 3(B2)). Intralipid (a) showed rare color pixels due to noise. The red GNR signal could be clearly visualized by itself (b) and when mixed with intralipid (c). The GNR aggregation layer at the test tube interface on top showed mostly red pixels with a few blue pixels.

To show detection of GNR which blue shifted the OCT signal, B-scan images of 0.1% intralipid and dilute GNR with SPR at 963 nm were taken on the 1050 nm swept-source OCT system. SLoW ratios were calculated as before, and histogram distribution plots of the SLoW ratios for the intralipid and GNR samples were generated (Fig. 5). The histograms were normalized to the total number of pixels in the B-scan which met the initial intensity threshold. Again, the intralipid showed a normal distribution centered on zero. The GNR, on the other hand, showed a SLoW ratio with a mean 3 SD more than that of the intralipid distribution. With a 3.09 SD or 0.9 dB SLoW ratio as the cutoff, the GNR signal could be

#224761 - $15.00 USD Received 10 Oct 2014; revised 14 Jan 2015; accepted 5 Feb 2015; published 11 Feb 2015
© 2015 OSA

cleanly separated from the intralipid signal. The spectral contrast for this sample, GNR, and OCT system combination was 3.

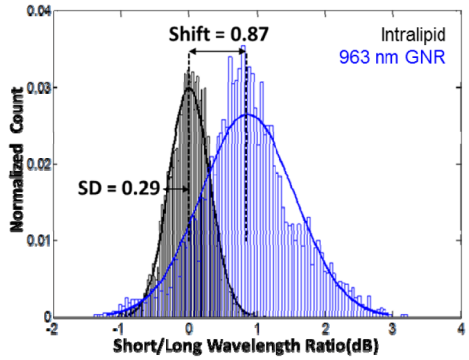

Fig. 5. Histogram distribution plots of the spectral shift of the OCT signal from 0.1% intralipid (tissue phantom) and dilute GNR with SPR at 963 nm. The signal's spectral shift was measured by the ratio between the intensity of short (<1050 nm) and long (>1050 nm) wavelength components of the OCT signal and converted to a dB scale. Intralipid (black) showed normal distributions centered on zero. The GNR showed a SLoW ratio with a mean 3 SD more than that of the intralipid distribution.

Using –0.9 and + 0.9 dB as cutoffs, we again color-coded the SLoW ratio information over the B-scan images. Blue was used to show the regions with SLoW ratios greater than 0.9 dB, and red was used to show the regions with SLoW ratios less than –0.9 dB. Due to speckle noise, the intralipid (Fig. 6(a)) showed a few colored pixels. The blue GNR signal could be clearly visualized (Fig. 6(b)). Specifically, 43% of the SLoW signal from the GNR sample was greater than 0.9 dB compared to only 0.1% from the intralipid sample.

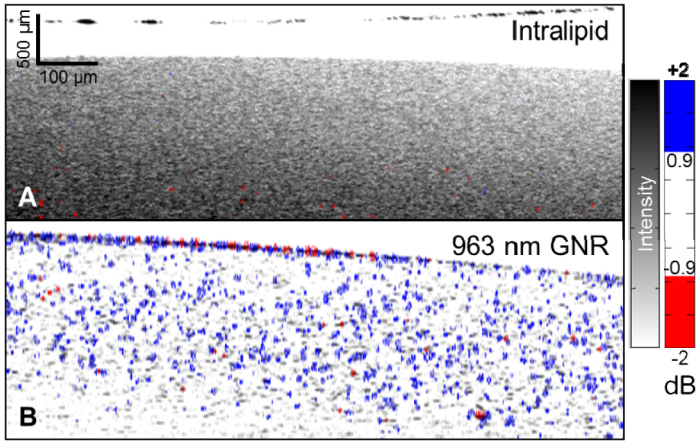

Fig. 6. OCT images of (a) 0.1% intralipid and (b) dilute GNR with SPR at 963 nm. The OCT signal intensity is shown on an inverse gray scale, and SLoW ratio information is color-coded with cutoffs set at ± 3.09 SD (± 0.9 dB) of the spectral distribution of intralipid (Fig. 5). Intralipid (a) showed sparse color pixels due to noise. The blue GNR signal (b) could be clearly visualized. A few red pixels are also seen in solution and in the aggregation layer at the test tube interface on top.

3.5 GNR detection in cultured cells

We then tested our detection methodology on cultured RPE cells suspended in 1% gelatin. B-scan images of 1% gelatin, unlabeled RPE cells, and RPE cells labeled with GNR coated with PEG and Tat were taken. The GNR used in this study were the 10 × 50 nm GNR that had

#224761 - $15.00 USD Received 10 Oct 2014; revised 14 Jan 2015; accepted 5 Feb 2015; published 11 Feb 2015
© 2015 OSA

SPR at 870 nm when coated with CTAB and at a concentration of 5×10^{10} nanorods/mL. Based on the SD of the SLoW histogram from unlabeled RPE cells, new cutoffs of −2 and + 2 dB were established for the experiment. Using this criterion, 5% of the SLoW signal from the GNR-labeled RPE cells was less than −2 dB. GNR-labeled RPE cells (Fig. 7(c)) could be distinguished (red dots), in sharp contrast with unlabeled cells (Fig. 7(b)). A few GNR-labeled cells unexpectedly showed blue, perhaps due to heterogeneity in GNR dimensions and SPR or the interaction of aggregated GNR closely localized in the same cell.

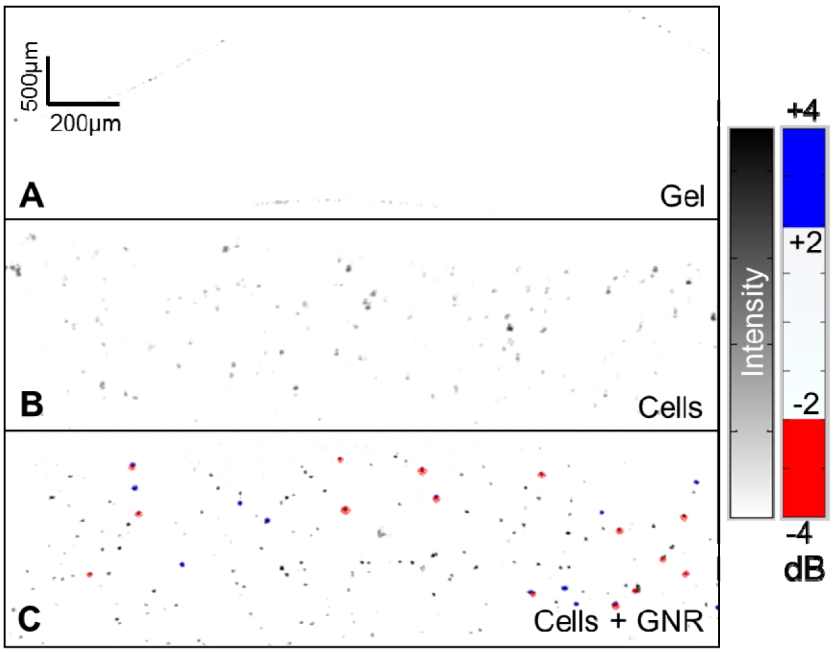

Fig. 7. OCT images of (a) 1% gelatin, (b) unlabeled cultured RPE cells, and (c) RPE cells labeled with GNR. The spectral shift of the backscattered/reflected OCT signal is shown as a SLoW ratio with a blue-white-red color scheme with cutoffs set at ± 3.09 SD (± 2 dB) of the spectral distribution of unlabeled cells. The intensity of the OCT signal is shown on an inverse gray scale. GNR-labeled RPE cells (c) could be distinguished by their spectral shift (red dots), in sharp contrast with unlabeled cells (b). A few GNR-labeled cells showed blue, most likely due to the spread in the GNR spectrum associated with GNR heterogeneity or aggregation.

3.6 Intrinsic spectral shifts in the human retina

The tissue of interest for the eventual application of this work is the human retina *in vivo*. Because the developed methodology relies on GNRs producing localized spectral shifts, we sought to assess for potential intrinsic spectral shifts in the human retina that may complicate detection. After processing and establishing cutoffs based on the spectral distribution of the human retina, we found a few pixels at the inner segment/outer segment junction (IS/OS) and the RPE with localized spectral shift associated with high signal intensity pixels (light blue and red dots in Fig. 8).

#224761 - $15.00 USD Received 10 Oct 2014; revised 14 Jan 2015; accepted 5 Feb 2015; published 11 Feb 2015
© 2015 OSA

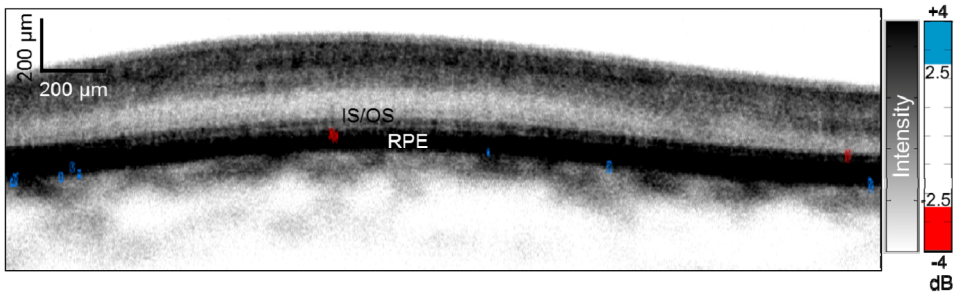

Fig. 8. OCT image of (unlabeled) human retina *in vivo*. The OCT signal intensity is shown on an inverse gray scale, and SLoW ratio information is color-coded with cutoffs set at ± 3.09 SD (± 2.5 dB) of the spectral distribution of retinal tissue. There were no areas of localized spectral shifts except at a few pixels between the inner segment/outer segment junction (IS/OS) and retinal pigment epithelium (RPE).

4. Discussion

OCT is an imaging technology that has yet to be able to take advantage of contrast agents capable of cellular and molecular labeling. If such a contrast agent could be found, then the high-resolution 3D volumetric imaging capability of OCT could be further extended to include a wider variety of biological investigations. Herein, we demonstrated the detection of GNR in tissue phantoms and RPE cells with an 840 nm commercial OCT system. Additionally, we showed the detection of GNR with SPR at 963 nm with a 1050 nm swept-source OCT system. Specifically, we found that GNR aggregates produced systemic red or blue shift of backscattered/reflected light that could be quantified as a SLoW ratio. The SloW ratio could then be used to distinguish the GNR from their surrounding environment. We furthermore defined the term spectral contrast which can be used to conceptualize and assess the effectiveness of any given GNR, sample, and OCT system combination.

This work extends previous OCT studies investigating the use of extrinsic contrast agents. Past approaches employed contrast agents as reflectance enhancers (scatterers) or reducers (absorbers). In the case of the former, because tissue reflectance usually spans a wide dynamic range due to variable incidence angle, speckle, and composition, reflectance itself may not provide sufficient contrast. In the case of strongly absorbing agents, OCT is used to detect the resulting "shadow" cast on subjacent tissue. While this is useful in establishing transverse location, absorbing agents are thought to produce a less sensitive and localized signal as compared to scattering agents in spectroscopic OCT [19]. While absorptive contrast could work well in labeling regions within turbid tissue with high concentrations of absorbers, it would not work well with our goal of labeling a sparse collection of cells within semitransparent retinal layers. In our situation, a reflective contrast agent that produced positive OCT signal at low concentration was needed.

Previous work have also described efficient spectroscopic algorithms [9, 20] which improved detection of absorptive contrast agents. These have superficial resemblance to the spectral fractionation algorithm described here, but there are important differences in their form and purpose. For example, the spectral triangulation algorithm by Yang et al. [9] tackled the problem that absorption and scattering both attenuate the OCT signal in a depth dependent fashion, and the absorption coefficient cannot be uniquely determined from measurement when the scattering coefficient is unknown. Spectroscopic OCT at 2 wavelengths generally cannot resolve the uncertain contribution of scattering. But by measuring at the absorption peak of a dye and 2 neighboring wavelengths, the effect of scattering can be canceled out because the scattering coefficient is approximately a first order function of wavelength (increasing linearly with shorter wavelengths). Fractionating the OCT spectrum beyond 3 would not further enhance this algorithm since the noise is a first order function of wavelength. Our problem is different because the desired signal is spectrally shifted scattering

#224761 - $15.00 USD Received 10 Oct 2014; revised 14 Jan 2015; accepted 5 Feb 2015; published 11 Feb 2015
© 2015 OSA

rather than absorption. The signal is the systematic shift of the reflectance spectrum due to GNR SPR, while the noise is random spectral shift due to speckle interference between nearby tissue (or phantom) structures. By fractionating the OCT spectrum into narrow sub-bands, depth resolution is sacrificed, but spectral speckle noise is suppressed by averaging over more spectral bands. In our spectral fractionation algorithm, fractionation into more narrow bands would further improve spectral contrast because the spectral reflectance noise is essentially random and not a first order function of wavelength. Thus in our spectral fractionation scheme, the spectral contrast enhancement would continue to scale with increasing subdivision of spectral sub-bands at the cost of further reduction in axial spatial resolution.

With regards to the use of GNR specifically, the signal enhancing effect of GNR has previously been demonstrated [21]. In addition, several groups have investigated the use of GNR as contrast agents in conjunction with additional instrumentation [22, 23]. More recently, a similar detection methodology was reported employing a dual wavelength-band swept-source OCT system [10]. In their case, the contrast was derived from the difference between the signals from widely separated spectral bands from 2 tunable lasers (1040 nm versus 1300 nm). The detection method described in this study enhances spectral contrast with the spectral fractionation algorithm and therefore does not require specialized hardware with 2 separate light sources. Thus our approach could be more readily implemented on any conventional Fourier-domain OCT system. The spectral fractionation algorithm significantly improved our ability to identify GNR by (1) decreasing the spectral shift noise in the background tissue and (2) increasing the spectral (SLoW ratio) shift in the OCT signal from GNR particle. The first effect derives from reduced speckle noise as a result of averaging sub-band B-scans with different speckle patterns. The second results from the change in how the sub-band splits overlap with the slope of the GNR extinction spectrum. We furthermore showed the detection of GNR coated with PEG and Tat that were internalized by RPE cells. To our knowledge, this is the first demonstration of the detection of cellular labeling using GNR and OCT.

Particle aggregation presents an opportunity and challenge to the developed GNR contrast agent detection scheme. Aggregation occurred in both the dilute suspension and labeled cells, which increased the backscattered signal intensity and helped with detection. With small aggregates in solution, a small systematic shift in peak of the extinction spectra was found, which did not interfere with detection using the spectral fractionation scheme. With larger aggregates in the labeled cells, inhomogenous spectral shifts were demonstrated by the presence of both red- and blue-shifted pixels in the same OCT images. This may be due random spectral shifts from speckle interference effects in large aggregates. Evidence of this effect was also found in the dense aggregate layer at the interface between GNR suspension and test tube wall *in vitro,* as well as in the RPE layer *in vivo*. In the RPE, this could be from melanin granules. Thus, the aggregation effects both enhance reflectance and produce spectral speckle noise. To produce the optimal contrast for labeled cells, it will be necessary to control the level of GNR uptake and level of aggregation through GNR surface coating and the incubation conditions. Further research is necessary to optimize the GNR design and the cell labeling procedures.

In terms of the spectral speckle noise in densely scattering tissue such as the RPE, several approaches could be used to increase contrast between the systematic GNR spectral shift and random spectral noise. First, a wider spectrum light source could be used to improve the spectral contrast between GNR and native tissue with a broad SLoW ratio distribution, like the RPE. To elaborate, the slope of the GNR extinction curve, which has the same shape as the reflectance/scattering curve [24, 25], within the OCT spectral window is a key determining factor of spectral contrast. The theoretical model predicts that capturing more of the GNR SPR slope within a wider OCT spectral window would lead to increased contrast. For example, increasing the 45 nm bandwidth of the 840 nm OCT system to 65 nm and

#224761 - $15.00 USD Received 10 Oct 2014; revised 14 Jan 2015; accepted 5 Feb 2015; published 11 Feb 2015
© 2015 OSA

fractionating into 4 sub-bands should increase the spectral contrast between the GNR (870 nm SPR) and intralipid by ~30%. Second, averaging of more B-scans taken at the same location could further suppress spectral noise and thereby improve the efficiency of detecting the GNR spectral signature. Finally, in the case of the RPE in the *in vivo* retinal OCT, significant spectral noise was only found in pixels with much higher OCT signal intensity than GNR-labeled RPE cells. Therefore, filtering out pixels with very high signal intensity is a viable strategy to suppress noise in this specific case.

5. Conclusion

We demonstrated a novel OCT contrast mechanism using spectral fractionation analysis and GNR with SPR tuned to one side of the OCT spectrum. Specifically, we showed that this technique could detect GNR in labeled cells *in vitro*. To our knowledge, this represents the first demonstration of a cellular contrast agent for OCT imaging.

Acknowledgments

This work was supported by NIH Grants R01EY023285, R01EY024544, R01EY023397, T32EY007135, T32EY23211, a grant from the Oregon Health & Science University Foundation, and an unrestricted grant from Research to Prevent Blindness. Financial interests: Yali Jia and David Huang have a significant financial interest in Optovue. David Huang also has a financial interest in Carl Zeiss Meditec. These potential conflicts of interest have been reviewed and managed by Oregon Health & Science University. Yali Jia, Gangjun Liu, Ashwath Jayagopal, and David Huang have potential patent interest in the subject of this article. Other authors do not have financial interest in the subject of this article.

© 2015 OSA